Relation between bank erosion and bed incision in the braided reach of the Lower Yellow River undergoing channel degradation

Xia, Junqiang; Cheng, Yifei; Zhou, Meirong; Yu, Xin; Xu, Xiangzhou; Blanckaert, Koen; Wang, Zhengbing

DOI
10.1016/j.ijsrc.2024.12.002

Publication date
2025

Document Version
Final published version

Published in
International Journal of Sediment Research

Citation (APA)
Xia, J., Cheng, Y., Zhou, M., Yu, X., Xu, X., Blanckaert, K., & Wang, Z. (2025). Relation between bank erosion and bed incision in the braided reach of the Lower Yellow River undergoing channel degradation. *International Journal of Sediment Research*, *40*(2), 241-252. https://doi.org/10.1016/j.ijsrc.2024.12.002

International Journal of Sediment Research 40 (2025) 241–252

Contents lists available at ScienceDirect

International Journal of Sediment Research

journal homepage: www.elsevier.com/locate/ijsrc

Original Research

Relation between bank erosion and bed incision in the braided reach of the Lower Yellow River undergoing channel degradation

Junqiang Xia [a,*], Yifei Cheng [a,*], Meirong Zhou [a], Xin Yu [b], Xiangzhou Xu [c], Koen Blanckaert [d], Zhengbing Wang [e]

[a] State Key Laboratory of Water Resources Engineering and Management, Wuhan University, Wuhan 430072, China
[b] Yellow River Institute of Hydraulic Research, Zhengzhou 450000, China
[c] School of Hydraulic Engineering, Dalian University of Technology, Dalian 116024, China
[d] Institute of Hydraulic Engineering and Water Resources Management, Research Unit Hydraulic Engineering and Environmental Hydromechanics, Technische Universität Wien (TU Wien), Vienna, Austria
[e] Department of Hydraulic Engineering, Faculty of Civil Engineering and Geosciences, Delft University of Technology, Delft, the Netherlands

A R T I C L E I N F O

Article history:
Received 29 February 2024
Received in revised form
11 November 2024
Accepted 12 December 2024
Available online 16 December 2024

Keywords:
Bank erosion
Bed incision
Bank erosion volume
Channel scour volume
Braided reach
Lower Yellow River (LYR)

A B S T R A C T

A general increase in the bankfull width and depth is found in downstream reaches because of upstream damming, especially in the braided reach of the Lower Yellow River (LYR), but the magnitude of bank erosion and its relation with bed incision remain little explored. Here based on long-term measured cross-sectional profiles (1999–2020), a quantitative method is proposed to estimate the bank erosion volume in the braided reach of the Lower Yellow River, with the contribution of bank erosion to the channel scour volume further determined. A quantitative relation was developed and calibrated between bank erosion width and bed incision depth, using the sediment continuity equation and measured data. The results indicate that: (i) significant bank erosion and bed incision processes are prevalent in the braided reach and its sub-reaches, with the bankfull widths increasing by 317–511 m and the bankfull depths increasing by 1.9–2.4 m in these reaches after the operation of the Xiaolangdi (XLD) Reservoir in 1999. Bank erosion has been dominant over bank accretion at more than 71% of the sections in the braided reach, with the most active bank deformation detected in the middle sub-reach. (ii) The cumulative bank erosion volumes temporally increased and spatially decreased, with the value of 1.80×10^8 m^3 in the upper sub-reach (R1), 1.52×10^8 m^3 in the middle sub-reach (R2), 1.08×10^8 m^3 in the lower sub-reach (R3), and 4.40×10^8 m^3 in the whole braided reach during the period of 1999–2020. Bank erosion contributed 33% of the cumulative channel scour volume in the braided reach, with a close relation developed between cumulative bank erosion volume and the previous 5-year average incoming sediment coefficient during flood seasons. (iii) A close inverse relation exists between bank erosion and bed incision in the whole braided reach and its sub-reaches, with the coefficients of determination greater than 0.90, which indicated that bank erosion hindered the process of bed incision. If there was no bank erosion after 1999, the cumulative bed incision depth would increase by at least 0.7 m in each reach. Furthermore, a similar quantitative relation was also applied to calculate the cumulative bed incision depth and bank erosion width in the braided reach during the period of 1960–1964 (the first stage after operation of the Sanmenxia Reservoir). Quite high accuracy was achieved in this analysis, with the coefficient of determination being equal to 0.96.

1. Introduction

Significant morphological changes take place in downstream reaches due to the alteration in hydrology and sediment dynamics imposed by upstream damming. The morphology evolution is influenced by the flow-sediment regime, bank material, river

* Corresponding authors.
E-mail addresses: xiajq@whu.edu.cn (J. Xia), chengyf@whu.edu.cn (Y. Cheng).
Peer review under the responsibility of International Research and Training Centre on Erosion and Sedimentation.

https://doi.org/10.1016/j.ijsrc.2024.12.002
1001-6279/

regulation works, vegetation, and other channel boundary conditions (Swanson et al., 2011). Frequent bank erosion, usually together with long-distance channel degradation, is extensively observed and is the principal type of channel adjustments in the downstream reaches with erodible bank material (Craddock et al., 2010; Latrubesse et al., 2017; Słowik et al., 2018; Walling & Fang, 2003; Williams et al., 2020). How the channel adapts and adjusts its geometry after dam construction is a core question. In addition, adverse ecologic or economic effects of bank erosion have been reported worldwide, with substantial losses in riparian zones, hydraulic structures adjacent to channels, and croplands (Florsheim et al., 2008; Yan et al., 2023). Due to detrimental effects of bank erosion, a large quantity of bank protection works has been constructed in rivers downstream of dams world-wide (Deng et al., 2022; Meade & Moody, 2010; Yang et al., 2015), and in the meantime the bed incision rate slows down (Miao et al., 2016). Therefore, it is of scientific and engineering significance to estimate the magnitudes of bank erosion and bed incision, and quantify their internal relation in fluvial processes especially for a large braided river in response to upstream damming.

Cross-sectional changes induced by dam construction have been qualitatively and quantitatively discussed in previous studies. Brandt (2000) extended the morphological relation proposed by Lane (1955) to predict the cross-sectional variations. As the discharge during the post-dam stage is less than that during the pre-dam stage, the widening and deepening processes of the main channel are anticipated when the incoming sediment concentration is less than the sediment transport capacity as described by Brandt (2000), which is also the common case for many downstream reaches. The braided reach located in the Lower Yellow River (LYR) is one of the most active river systems with an unstable main channel and erodible banks, the cross-sectional changes of which have attracted much more attention especially after the Xiaolangdi (XLD) Reservoir became operational in 1999. Ma et al. (2012) found a general increase in the bankfull width and depth at the Huayuankou (HYK) station in the braided reach of the LYR in 1999–2006. Xia et al. (2014) calculated the reach-scale bankfull width and depth of the braided reach, and these reach-scale parameters also increased remarkably in 1999–2012.

An important method to calculate the variation in bankfull channel dimensions (width, depth, and area) has been proposed based on the exponential decay function. Previous studies have investigated the morphological changes in rivers downstream of dams based on this method (Richard et al., 2005; Shin & Julien, 2010; Wu et al., 2008), which involves the determination of channel dimensions under the equilibrium state. Due to the uncertainty and complexity in determination of an equilibrium state, some researchers directly established some empirical formulas between the bankfull width or depth and the flow-sediment regime (e.g., incoming sediment coefficient and discharge) during flood seasons, according to the principle of the delayed response theory (Bi et al., 2019; Li et al., 2021; Wu et al., 2008; Xia et al., 2014). This type of method is feasible for the prediction of the channel adjustments. However little attention has been paid to the estimation of the bank erosion volume using these measured cross-sectional profiles, and the internal relation has not been quantified between bank erosion and bed incision.

Current methods to estimate bank erosion volume, include some refined field monitoring methods, various bank erosion models such as the bank stability and toe erosion model (BSTEM) (Arnez Ferrel et al., 2018; Darby et al., 2007; Klavon et al., 2017), and remote sensing images (Boardman, 2016; Fisher et al., 2013; Rowland et al., 2016). However, refined field monitoring methods such as the implementation of erosion pins, multibeam echo sounding-terresrial laser scanning (MBES-TLS) and real time kinematic global positioning system (RTK-GPS) monitoring, are often used in bank erosion observations in a small channel or a local reach of a large river (Fox et al., 2016; Leyland et al., 2017; O'Neal & Pizzuto, 2011; Yan et al., 2023; Zhang et al., 2019). The use of bank erosion models requires detailed flow and bank material data (Zhang et al., 2019). Some studies have attempted to make estimates of bank erosion volume together with sensing images and light detection and ranging (LiDAR) data or arctic digital elevation model (DEM) from which bank heights can be derived (Basumatary et al., 2021; Payne et al., 2017; Spiekermann et al., 2017; Williams et al., 2020). However, the applicability of LiDAR and TLS methods is undermined by data availability due to the uncertainty caused by complex data manipulation. To date, studies on long-term bank erosion observations in large rivers are limited to the analysis of remotely sensed imagery. As a matter of fact, it is also a choice to investigate bank deformation processes based on the measured cross-sectional profiles due to the high resolution, if regular measurements of cross-sectional profiles have been conducted in a specified alluvial river.

An alluvial river will experience a non-reversible series of channel adjustments once it is disrupted. Regime theory has been developed to describe the determined relation between bankfull depth and width under a relative equilibrium state, with many formulas proposed (Huang & Nanson, 2000; Millar, 2005). However, regime theory is inapplicable to a river reach under a non-equilibrium state. Some studies have attempted to quantify the relation between bank deformation and bed incision using some coupled mathematical models or empirical relations (Li et al., 2021; Xu & Shi, 1995; Zhou, 1992). Zhou (1992) established a quantitative relation between bed incision depth and bank erosion width at a section-scale in the braided reach of the LYR based on the cross-sectional profiles in 1960–1964. Some coupled one-dimensional models have been recently proposed to simulate both bed evolution and bank erosion processes (Asahi et al., 2013; Darby et al., 2007; Deng et al., 2019; Wang et al., 2022), but the applicability of these models is limited owing to the long computational time and uncertainty in simulating long-term channel evolution processes. Obviously, current methods are not accurate enough to investigate the relation between bank erosion and bed incision in an entire braided reach.

The braided reach in the LYR with erodible banks has experienced severe bank erosion and accretion throughout history. About 300 km^2 of floodplain area was eroded over 4 years owing to the operation of the Sanmenxia (SMX) Reservoir beginning in 1960 (Ma et al., 2012). The operation of the XLD Reservoir since 1999 has greatly altered the downstream flow and sediment regime over a relatively short period of time. Significant bank erosion and bed incision have occurred in the braided reach over the past 20 years, although considerable bank protection works have been constructed. Abundant measurements of cross-sectional topography have been collected in this reach. Yet, to the authors' knowledge, few studies have previously revealed the magnitude of bank erosion and its relation with bed incision in such a large braided river in response to upstream damming. As a consequence, the braided reach is selected as the study reach to do a detailed analysis of the magnitude and contribution of bank erosion to channel evolution, as well as the relation between bank erosion and bed incision during the post-dam stage. In the current study, the specific aims are to: (i) estimate the magnitude and process of bank erosion, as well as the delivery of bank sediment to the channel over the past 20 years based on the measured cross-sectional profiles; (ii) quantify the effect of bank erosion on bed incision by theoretically establishing a predictive relation between bed incision depth and bank erosion width using the equation of sediment continuity, in order to elucidate how the bed incision process will develop without the occurrence of bank erosion.

2. Study area and methodology

2.1. Description of braided reach

The Yellow River ranks the second longest river in China, with a length of 5464 km and a drainage area of 795,000 km^2. Originating from the Tibetan Plateau and flowing eastward through nine provinces before entering the Bohai Sea (Fig. 1(a)), the Yellow River is usually divided into upper (UYR), middle (MYR), and lower reaches (LYR). The lower reach, i.e., the Lower Yellow River, refers to the sector between Mengjin in Henan Province and Lijin in Shandong Province, with a length of 756 km. According to morphological characteristics, the reach upstream of Gaocun (GC) belongs to the braided reach (Fig. 1(b)), and three hydrometric stations are located in the reach, i.e., HYK, Jiahetan (JHT), and GC. This reach is characterized by highly unstable floodplain banklines, rapid migration of mainstream, and diverse channel widths along the reach. There are extensive floodplains on both sides of the main channel, which are utilized by local inhabitants, and the area of floodplains accounts for over 80% of the whole reach. Three hydrometric stations divide the braided reach into three sub-reaches: the reach upstream of HYK (R1), the reach between HYK and JHT (R2), and the reach between JHT and GC (R3) (Fig. 1(b)).

To consider the variation in the flow-sediment regime entering LYR, the relevant hydrological data were collected from the Yellower River Conservancy Commission (YRCC) (http://www.yrcc.gov.cn/). According to the operation of key reservoirs, four stages are commonly delineated to describe the variations in the supply of water and sediment in LYR. The flow and sediment regime entering the study reach can be represented by the data at the hydrometric station of HYK, covering the volumes of water and sediment from the mainstream and two tributaries. In terms of the variation in

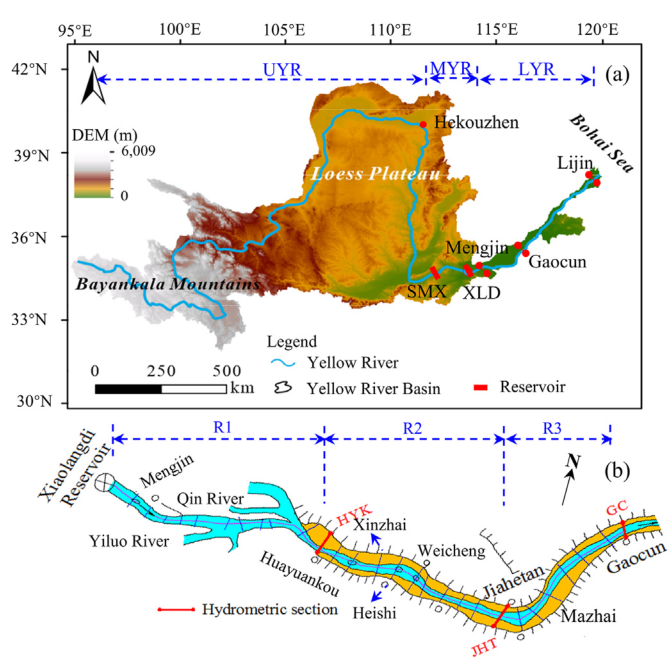

Fig. 1. (a) Yellow River Basin. (b) Braided reach of Lower Yellow River.

water volume, the water discharge at HYK slightly varied before 1986 (Fig. 2(a)), with an average annual water volume of 458×10^8 m^3 /y during the period 1951–1960 (before the operation of the SMX Reservoir) and 1960–1986 (after the operation of the SMX Reservoir). The incoming water volume suddenly decreased by 39% during the period 1986–1999 (around 279×10^8 m^3/y) due to the significant water resources development by a joint operation of the SMX Reservoir with other reservoirs in the UYR. After the operation of the XLD Reservoir, the incoming water volume slightly changed, with an average annual water volume of 278×10^8 m^3/y during the period of 1999–2020. In terms of the variation in sediment load, a general reduction existed at different stages. The incoming sediment amount was the maximum during the period of 1951–1960, with an average value of 14.6×10^8 t/y. The later periods witnessed a decrease, with an average incoming sediment amount of 11.2×10^8 in 1960–1986 and 6.9×10^8 t/y in 1986–1999 due to the reservoir operation and soil conservation measures in the MYR drainage basin (the Loess Plateau). The XLD Reservoir with a designed capacity of 12.7 km^3 exerted a powerful control on the sediment release. The sediment amount at HYK sharply decreased by 90%, with an average value of 1.2×10^8 t/y during the period 1999–2020. The incoming annual sediment amount was less than 0.1×10^8 t even in some years (2015–2017).

The channel evolution processes in the braided reach were closely related to the variation in the flow and sediment regimes. Fig. 2(b) shows the temporal variations in cumulative channel evolution volumes of LYR and the braided reach, which were calculated based on the topography method by YRCC. The channel of LYR continuously aggraded before the operation of the XLD Reservoir except for two short periods of 1960–1964 and 1980–1985. The cumulative channel deposition volume reached the maximum value of 55.78×10^8 m^3 in LYR and of 33.47×10^8 m^3 in the braided reach during the period of 1950–1999. Considerable channel degradation occurred after the operation of the XLD Reservoir, with the total channel scour volume of 20.00×10^8 m^3 in LYR. The braided reach was prominently eroded, with the total scour volume of 13.38×10^8 m^3, which accounted for about 67% of the total channel scour volume in the entire LYR.

Repeated surveys of cross-sectional profiles indicate that channel widening owing to bank erosion has been extremely prominent in the braided reach. The variations in cross-sectional profiles are shown in Fig. 3, with significant bank erosion and bed incision processes occurring at different sections. The floodplain banks are susceptible to erode on both sides, with the width of bank erosion even larger than 2,400 m at a specified section over the past 20 years (Fig. 3(b)). The process of bank erosion in the braided reach is closely linked to the composition of bank soil and mechanical properties. Previous studies (Xia et al., 2008) have indicated that the bank soil is vertically stratified in the braided reach. The surface layer is generally composed of low liquid limit clay, while the lower layer is silty or fine-grained. Remarkable variation exists in the clay content of bank soil along the reach, with the clay proportion varying from 3% to 35% in the surface layer and from 1% to 23% in the lower layer (Xia et al., 2008). The lower layer with minor clay is prone to fluvial erosion, and the surface layer of bank soil is easy to collapse as the shear strength is reduced by an increase in water content.

2.2. Methodology

Detailed methods are given for the estimation of the bank erosion volume and the quantification of the relation between bank erosion and bed incision. It should be noted that regular measurements of cross-sectional topography are necessary to utilize the following methods. For large rivers such as the Yellow

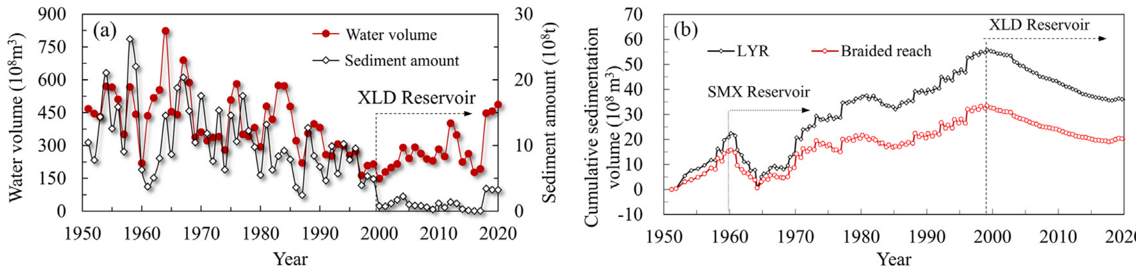

Fig. 2. Temporal variations in incoming flow-sediment regime and channel evolution volume: (a) incoming flow-sediment condition; (b) cumulative channel evolution volumes of braided reach and LYR.

River and the Yangtze River, regular measurements of topography can be obtained, while these methods are not applicable to rivers without measured topography. Measurements of cross-sectional profiles have been done by YRCC since the 1950s (Wang et al., 2017). Repeated surveys have been done twice a year, prior to and after the flood season from July to October at fixed sites which are called sedimentation sections (Wu et al., 2008). The number of sedimentation sections increased as the measurement techniques became mature. The total number of sedimentation sections increased from 91 (among which 28 sections were in the braided reach) in 1999 to 333 in 2004 (among which 147 sections were in the braided reach). To keep the consistency of the number of cross sections, the cross-sectional profiles were collected at the original 28 sedimentation sections in the braided reach.

2.2.1. Estimation of bank erosion volume

The procedure to estimate the bank erosion volume based on the measured cross-sectional profiles includes: the determination of reach-scale bankfull channel dimensions, the calculation of cumulative bank erosion width and bed incision depth, and the calculation of bank erosion volume.

1) Determination of reach-scale bankfull channel dimensions

Bankfull channel dimensions involve the width, depth, and area at the bankfull stage, which are usually used to describe the channel geometry in the analysis of fluvial processes and fluvial geomorphology (Harman et al., 2008; Leopold & Maddock, 1953; Wilkerson et al., 2014; Xia et al., 2014). Among these bankfull channel dimensions, the bankfull width and depth are critically important in the view of calculating the bank erosion volume. A few rules proposed by Xia et al. (2014) are utilized to determine the bankfull channel dimensions at a section, which emphasize the performance of farm dikes and the importance of referring to the previous location when the floodplain lips on both sides are not easily recognized. The cross-sectional profile at JHT is selected as an example to illustrate the procedure (Fig. 4). Compared with the previous observations, the point L and R (the square points) are, respectively, regarded as the lip of the floodplain on the left side (with the bed level of 75.8 m) and the right floodplain lip (74.8 m), among which the lower elevation is taken as the bankfull level. Then the width between these two lips is defined as the bankfull width (B_{bf}), and the main channel area under the bankfull level is the bankfull cross-sectional area (A_{bf}), with the bankfull depth (H_{bf}) being equal to the ratio of A_{bf} to B_{bf}.

Due to the complex variation in bankfull channel dimensions at different sections, the reach-averaged method proposed by Xia et al. (2014) is utilized, which can guarantee the continuity of the channel dimensions and flow condition (Eq. (1)):

$$\overline{G}_{\mathrm{bf}} = \exp\left(\frac{1}{2L}\sum_{i=1}^{N-1}\left(\ln G_{\mathrm{bf}}^{i+1} + \ln G_{\mathrm{bf}}^{i}\right) \times \Delta x_i\right) \quad (1)$$

where $\overline{G}_{\mathrm{bf}}$ is the reach-scale bankfull channel dimensions covering bankfull width, depth, and area; G_{bf}^{i} and G_{bf}^{i+1} are the channel dimensions at the ith and $(i+1)$th sections; L is the length of the study reach; Δx_i is the spacing between the ith section and $(i+1)$th section; N is the total number of sedimentation sections in the study reach. Based on the collected cross-sectional profiles at 28 sedimentation sections from YRCC during the period of 1999–2020, the reach-scale bankfull width and depth can be obtained during the period of 1999–2020. To illustrate the influences of different numbers of sedimentation sections on the calculation of reach-scale bankfull channel dimensions, the measurements of cross-sectional profiles were collected at 147 sections in 2018–2020. The relative errors of calculated reach-scale bankfull width and depth were commonly less than 10%. For example, the calculated reach-scale bankfull width and depth were 1,342 and 3.5 m in 2020 when the total number was 147, and the corresponding values were 1369 and 3.7 m when the total number was 28.

2) Calculation of cumulative bank erosion width and bed incision depth

Although the occurrence of bank erosion and accretion at a section is subject to uncertainty, a general channel widening process has been observed at reach-scale since the operation of Xiaolangdi Reservoir (Xia et al., 2014). Fig. 5 generalizes the adjustment process of channel geometry at reach-scale, with an assumption that bank erosion takes place on both sides. Then the cumulative bank erosion width and bed incision depth can be calculated by Eq. (2):

$$2\Delta B = \overline{B}_{\mathrm{bf}n} - \overline{B}_{\mathrm{bf}1}, \Delta H = \overline{H}_{bfn} - \overline{H}_{\mathrm{bf}1} \quad (2)$$

where $\overline{B}_{\mathrm{bf}1}$ and $\overline{H}_{\mathrm{bf}1}$ are the reach-scale bankfull width and depth after the flood season in 1999, respectively (m); $\overline{B}_{\mathrm{bf}n}$ and $\overline{H}_{\mathrm{bf}n}$ are the reach-scale bankfull width and depth after the flood season in the nth year after 1999 (m); $2\Delta B$ and ΔH are the cumulative bank erosion width and bed incision depth in n years after the XLD Reservoir operation, respectively (m).

3) Estimation of bank erosion volume

It is assumed that the wide and shallow cross-sectional geometry in a long reach is generalized into a rectangle. The bank erosion volume of the long reach is the product of bank erosion volume per unit river length and the length of the study reach. As shown in

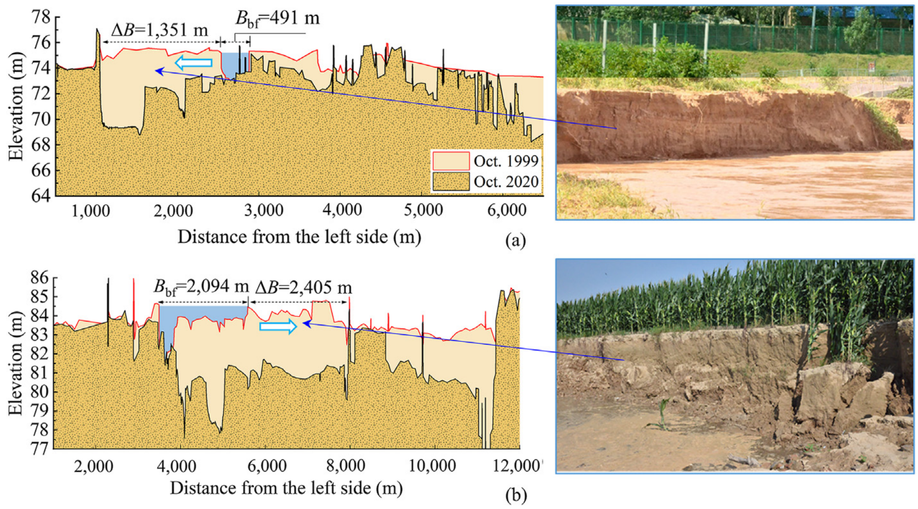

Fig. 3. Cross-sectional profiles at typical sections of: (a) JHT and (b) Weicheng.

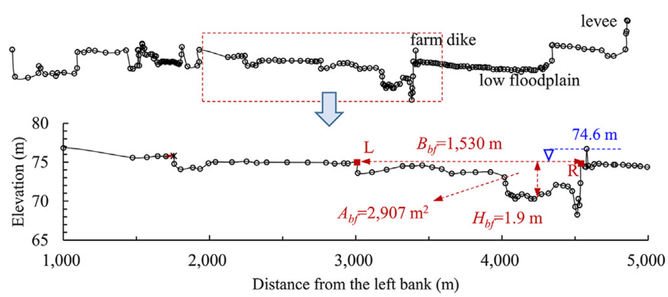

Fig. 4. Determination of bankfull channel dimensions at a typical sedimentation section.

Fig. 5, the bank erosion volume per unit length in n years is the product of bank erosion area per unit length and bank height. The bank erosion area per unit length is the product of the bank erosion width ($2\Delta B$) and unit length (1 m). The bank height can be estimated by the bankfull depth ($\overline{H}_{\mathrm{bf}n}$), which also includes the bed incision depth. Therefore, the bank erosion volume per unit length in n years can be represented by $\Delta V_{\mathrm{per}} = (\overline{B}_{\mathrm{bf}n} - \overline{B}_{\mathrm{bf1}}) \times 1 \times \overline{H}_{\mathrm{bf}n} = 2\Delta B\overline{H}_{\mathrm{bf}n}$. Then the bank erosion volume of the study reach can be obtained (Eq. (3)):

$$\Delta V_{\mathrm{bk}} = \Delta V_{\mathrm{per}} \times L \tag{3}$$

where the length, L, is 103.2 km for Reach R1, 100.8 km for Reach R2, and 77.1 km for Reach R3; ΔV_{bk} is the cumulative bank erosion volume of the different reaches (10^8 m^3). Because of regular measurements of cross-sectional profiles, this method ignores the detailed bank deformation process at a specific section, which is able to conveniently give an estimate of bank erosion volume in a long reach.

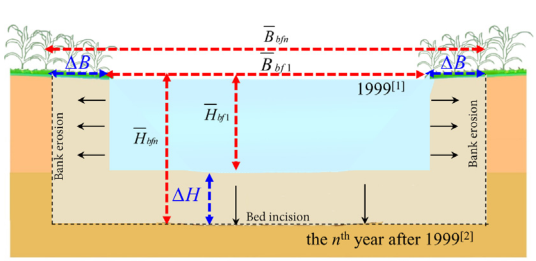

Fig. 5. Sketch showing variation in reach-scale bankfull channel geometry of braided reach.

2.2.2. *Quantitative relation between cumulative bed incision depth and bank erosion width*

The sediment continuity equation in steady flow indicates that the channel evolution is the result of the spatial variation in sediment discharge. For LYR undergoing channel degradation, the channel evolution included the deformation of the main-channel bed and floodplain banks. Therefore, the sediment continuity equation provides the rationale of lateral and vertical changes in the main channel, which is utilized to analyze the relation between bed incision and bank erosion (Eq. (4)):

$$\rho' \frac{\partial A_0}{\partial t} = -\frac{\partial QS}{\partial x} \tag{4}$$

where A_0 denotes the channel evolution area in a specified period, including the deformations of the main-channel bed and floodplain banks; Q and S are the discharge and sediment concentration, respectively; t is the time; x is the longitudinal distance; ρ' is the dry density of the bed material.

Eq. (4) can be further written as Eq. (5):

$$\rho' \frac{\partial A_0}{\partial t} = \rho' \frac{A_2 - A_1}{\Delta t}, \frac{\partial QS}{\partial x} = \frac{(QS)_{\mathrm{out}} - (QS)_{\mathrm{in}}}{\Delta x} \tag{5}$$

where $(QS)_{\mathrm{out}}$ and $(QS)_{\mathrm{in}}$ denotes the sediment discharge at the outlet and inlet; A_1 and A_2 denotes the bankfull area at the initial and ending times, respectively; Δt and Δx are the temporal and longitudinal steps, respectively. The cross section is sketched into a rounded trapezoid, with the adjustment processes of channel geometry outlined in Fig. 5. The corresponding bankfull area in Eq. (5) can be written as Eq. (6):

$$\begin{aligned} A_1 &= \overline{B}_{\mathrm{bf1}}\overline{H}_{\mathrm{bf1}} \text{ (bankfull area in the previous year)} \\ A_2 &= \left(\overline{B}_{\mathrm{bf1}} + 2\Delta B\right)\left(\overline{H}_{\mathrm{bf1}} + \Delta H\right) \text{ (bankfull area in the later year)} \end{aligned} \tag{6}$$

where $2\Delta B$ and ΔH have the same meaning as Eq. (2).

Substituting Eqs. (5) and (6) into Eq. (4), the bed incision depth can be estimated as Eq. (7):

$$\Delta H = \left[\frac{\Delta t}{\rho' \Delta x}(Q_{\text{in}}S_{\text{in}} - Q_{\text{out}}S_{\text{out}}) - 2\Delta B\overline{H}_{\text{bf1}}\right] \bigg/ \left(\overline{B}_{\text{bf1}} + 2\Delta B\right)$$
$$= \underbrace{\left[\frac{\Delta t}{\overline{B}_{\text{bf1}} + 2\Delta B} \frac{(Q_{\text{in}}S_{\text{in}} - Q_{\text{out}}S_{\text{out}})}{\rho' \Delta x}\right]}_{\text{term I}} + \underbrace{\frac{\overline{H}_{\text{bf1}}\overline{B}_{\text{bf1}}}{\overline{B}_{\text{bf1}} + 2\Delta B} - \overline{H}_{\text{bf1}}}_{\text{term II}} \quad (7)$$

where Δt is the cumulative years since 1999; Δx is the length of a study reach; Q_{in} and S_{in} are the annual mean discharge and sediment concentration at the inlet; Q_{out} and S_{out} are the annual mean discharge and sediment concentration at the outlet; herein the term $\Delta t/(\overline{B}_{\text{bf1}} + 2\Delta B)$ (written as K_{B} in the following analysis) is defined as the reciprocal inverse of the variation rate of the bankfull width, which is not a constant value and varies with time. When bank erosion continuously occurs in a study reach, indicating an increasing ΔB, both terms I and II in Eq. (7) decrease, which will result in a reduction in the value of the bed incision depth. Therefore, the process of channel widening will hinder the process of bed incision.

The spatial variation in sediment discharge $((Q_{\text{in}}S_{\text{in}} - Q_{\text{out}}S_{\text{out}})/(\rho' \Delta x))$ represents the channel evolution volume per unit length and varies with time in the term I, which is hard to obtain in a local reach with a lack of hydrometric stations. While determining the parameters in Eq. (7), an assumption is made that the channel evolution volume per unit length is closely related to the variation rate of bankfull width (K_{B}), and consequently the value of the term I is a function of K_{B}, which means that $\frac{\Delta t}{\overline{B}_{\text{bf1}} + 2\Delta B} \frac{(Q_{\text{in}}S_{\text{in}} - Q_{\text{out}}S_{\text{out}})}{\rho' \Delta x} = f(K_{\text{B}})$. Then Eq. (7) can be finally written as Eq. (8):

$$\Delta H = f(K_{\text{B}}) + \frac{\overline{H}_{\text{bf1}}\overline{B}_{\text{bf1}}}{\overline{B}_{\text{bf1}} + 2\Delta B} - \overline{H}_{\text{bf1}} \quad (8)$$

3. Recent variations in bank erosion and bed incision

The reach-scale bankfull channel dimensions covering bankfull width and depth of different reaches were determined from 1999 to 2020, which can give a full description of the channel adjustment processes in the braided reach in response to upstream damming. The cumulative bank erosion width and bed incision depth were then obtained using Eq. (2). Consequently, the temporal variations in the bank erosion volume of different reaches were quantified.

3.1. *Characteristics of channel adjustments*

The channel adjustments were characterized by the coexistence of widening and incision in the braided reach after the operation of the XLD Reservoir (Fig. 6). The increase in the reach-scale bankfull width and depth was closely related to the released sediment concentration. As shown in Fig. 2, the incoming sediment load significantly was reduced by around 90%, which became smaller than the sediment transport capacity. Previous studies have also indicated that the hydraulic shear stress was one order larger than the critical shear stress of bank soil in the braided reach (Xia et al., 2008). Therefore, a significant increase could be found in the reach-scale bankfull width and depth. However, the increase in the reach-scale bankfull width and depth was not monotonic in each sub-reach from 1999 to 2020, with the increase rate reducing after 2012, which resulted from the adjustments of the channel boundary conditions.

The bed material became coarsened in the braided reach, and the sediment transport capacity became smaller due to the wide and deep main channel. In addition, the construction of bank protection works also reduced the increase of bankfull width to some extent. A minor decline occurred in the bankfull width of Reach R2 from 2011 to 2015, which suggested that the process of bank accretion was dominant in some years. In general, the reach-scale bankfull width in 2020 increased by 48% in Reach R1, 38% in Reach R2, and 52% in Reach R3. The reach-scale bankfull width of the braided reach evidently increased from 943 m in 1999 to 1,369 m in 2020, which, however, reduced slightly during the period of 2015–2017. These three years featured extremely small discharge and sediment load (Fig. 2(a)), with the average discharge lower than 835 m^3/s during the flood seasons. The low flow was concentrated in the deep channel, and there was no chance for the point bars on both sides to submerge during an entire hydrological year. As a consequence, these point bars were classified into floodplain zones when determining the bankfull level (Fig. 7). This treatment is accountable to a slight decline in the bankfull width in the braided reach.

The variation in the bankfull depth is closely linked to the channel evolution processes. Continuous channel degradation occurred in the braided reach and its sub-reaches from 1999 to 2018, and consequently the bankfull depth of each reach continually increased during this period. Heavy sediment deposition took place in the braided reach in 2019 due to the large incoming sediment load released by the XLD Reservoir, with the annual deposition volume of 0.64×10^8 m^3 in Reach R1, 0.40×10^8 m^3 in Reach R2, 0.04×10^8 m^3 in Reach R3, and 1.08×10^8 m^3 in the entire braided reach, which decreased the reach-scale bankfull depth of each reach in this year, as shown in Fig. 6(b). Generally, the reach-scale bankfull depth considerably increased in each sub-reach during the post-dam stage, with an increase by 1.9 m in Reach R1, 2.1 m in Reach R2, and 2.4 m in Reach R3. The bankfull depth of the entire braided reach was 3.7 m in 2020.

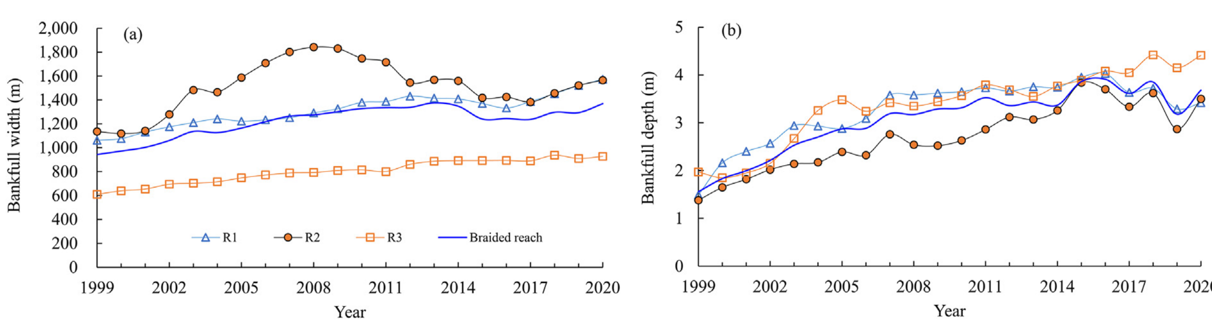

Fig. 6. Temporal variations in bankfull width and depth of different reaches: (a) bankfull width and (b) bankfull depth.

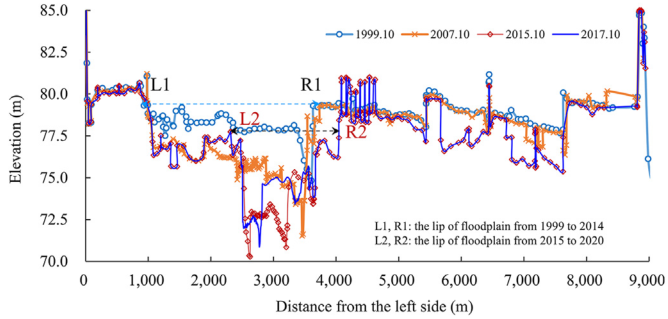

Fig. 7. Adjustment in determination of main channel at Gucheng section in response to low discharges from 2015 to 2017.

Two common time-series prediction models, including the Holt−Winters model (Hyndman & Athanasopoulos, 2018; Winters, 1960) and the autoregressive integrated moving average (ARIMA) model (Hyndman & Athanasopoulos, 2018), were used to predict the variations in bankfull width in the subsequent 10 years, by taking the entire braided reach as an example (Fig. 8(a)). It is indicated that a continual and steady increase will exist in the bankfull width. It is not reasonable to predict the variation trends of incoming sediment amount in the future simply by the time-series prediction models, and therefore the temporal variation in incoming sediment amount from 1999 to 2020 has been presented in Fig. 8(a). It can be found that the incoming sediment amount gradually increased from 2000 to 2004, slightly increased from 2011 to 2012, and then increased to a large value from 2018 to 2020. However, the bankfull width will decrease according to the self-adjustment principle of fluvial processes, when the incoming sediment amount significantly increases and water volume slightly varies in the future. Therefore, it is not reliable to analyze the variation in bankfull width without considering the influences of flow regime and engineering works.

3.2. Characteristics of bank erosion and bed incision

3.2.1. Cumulative bank erosion width and bed incision depth

Spatial variations in the cumulative bank erosion width and bed incision depth can help to identify the vulnerable zone which experiences the most prominent channel adjustments. The cumulative bank erosion width and bed incision depth along the reach during the period of 1999−2020 are presented in Fig. 9, where a positive value indicates bank erosion or bed incision. In terms of the spatial variation in cumulative bank erosion width, bank erosion is a common phenomenon at most sections during the post-dam stage. Only four sections experienced prominent bank accretion, with the cumulative bank accretion width larger than 100 m. There were some sections in Reach R1 with stable banks and strong anti-erosion properties, and therefore, a slight magnitude of bank erosion or accretion occurred in these sections. The bank deformation process was the most prominent in Reach R2 among the three sub-reaches. Both the strongest bank erosion and accretion activities were detected in Reach R2, with the largest accretion width of 1,146 m in the section at Xinzhai and the largest erosion width of 2,654 m in the section at Heishi (these locations are shown in Fig. 1). Bank erosion commonly occurred at the majority of sections in Reach R3, with relatively small magnitudes. However, several sections also experienced drastic bank erosion, with the cumulative bank erosion width exceeding 1,000 m. In terms of the spatial variation in cumulative bed incision depth, all the sections were substantially incised except the section at Mazhai (the location is shown in Fig. 1), where the bed was cumulatively aggraded by 0.2 m. Although a significant difference existed in the magnitude of bed incision along the braided reach, a similarity was found in the variation ranges of cumulative bed incision depth in different reaches, which varied in the ranges of 0.7−3.1 m in Reach R1, 0.8−3.2 m in Reach R2, and 1.5−3.3 m in Reach R3.

3.2.2. Bank erosion volume and its contribution to channel evolution

Bank erosion volumes in the braided reach and its sub-reaches are shown in Fig. 10(a). It can be concluded from Fig. 10(a) that the magnitude of the bank erosion volume generally increased in each reach after the operation of the XLD Reservoir. A slight reduction in the bank erosion volume of the braided reach during the period of 2015−2017 was also the result of the reduction in bankfull width as previously mentioned. A large difference can be found in the variation in the bank erosion volume of different reaches. The process of bank erosion was prevalent in Reach R1, and the bank erosion volume significantly increased with time in this reach. The Reach R2 was characterized by active processes of bank erosion and accretion, leading to a fluctuation in bank erosion volume in some years. A gradual increase occurred in the bank erosion volume of Reach R3, while the cumulative bank erosion volume was the smallest due to the highest stability in bank slope among the three sub-reaches. The cumulative bank erosion volume after the 2020 flood season summed up to 1.80×10^8 m^3 in Reach R1, 1.52×10^8 m^3 in Reach R2, 1.08×10^8 m^3 in Reach R3, and 4.40×10^8 m^3 in the braided reach. The bank erosion volumes in Reaches R1, R2 and R3 accounted for 41%, 34%, and 25% of the total value in the whole braided reach, respectively. The annual bank erosion volume per unit length in each sub-reach was 8.29×10^4, 7.19×10^4, and 6.67×10^4 m^3/(km·y), respectively. Time-series prediction models were also used to predict the variation in bank erosion volume in the entire braided reach

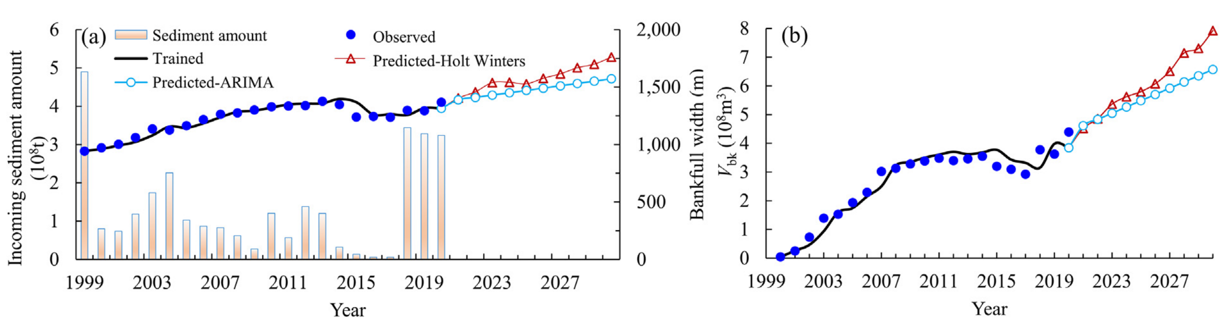

Fig. 8. Variations in bankfull width and bank erosion volume of the entire braided reach using the Holt−Winters and ARIMA models: (a) bankfull width and (b) bank erosion volume.

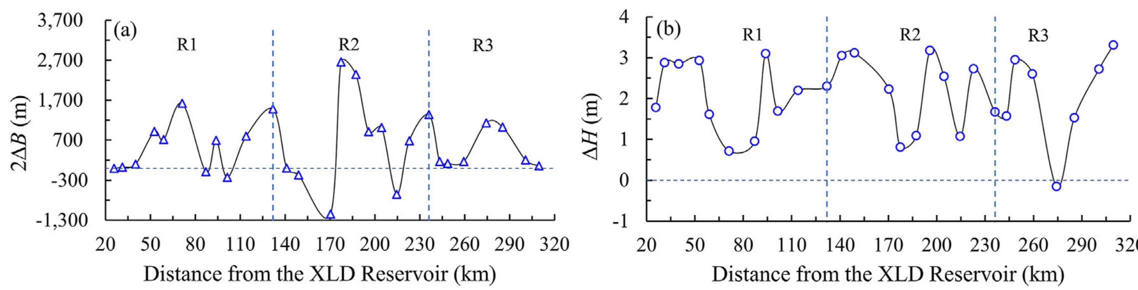

Fig. 9. Spatial variations in cumulative bank erosion width ($2\Delta B$) and bed incision depth (ΔH) along braided reach from 1999 to 2020: (a) cumulative bank erosion width and (b) cumulative bed incision depth.

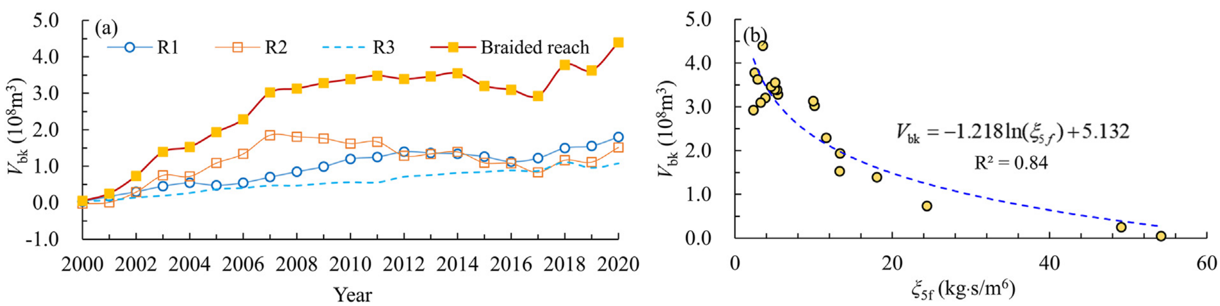

Fig. 10. Variations in bank erosion volume (V_{bk}) of the braided reach: (a) temporal variation and (b) effect of flow-sediment condition.

(Fig. 8(b)). Similar to the prediction of bankfull width, a continual and steady increase was also predicted during the later years. While the increase would be definitely hindered or slowed in the future, owing to the existence of river training works.

Fluvial erosion including bank erosion and bed incision plays an important role in sediment transport process. Previous studies found that a high rate of bank erosion will greatly influence the morphological stability especially in an extensive braided river system (Nandi et al., 2022). It remains uncertain to what extent the bank erosion process contributed to the channel evolution process of such a large braided river. On the basis of the bank erosion volume and the channel evolution volume calculated by the topography method, it is easy and more accurate to clarify the contribution of bank erosion. Around 33% of the total channel evolution volume during the period of 1999–2020 was supplied from bank erosion in the entire braided reach, which is equal to the ratio of cumulative bank erosion volume (4.40×10^8 m^3) to the total channel scour volume (13.38×10^8 m^3). Previous studies determined that the annual bank erosion volume per unit length was around 6.67×10^4 m^3/(km·y) in the Middle Yangtze River (Deng et al., 2022) and 6.99×10^4 m^3/(km·y) in a braided reach of the Hanjiang River with a length of 130 km (Xu & Shi, 1995). It is fairly rare in the global river systems to discover that the contribution induced by bank erosion was as dominant in the channel evolution process as in the large braided reach of LYR.

Some factors such as the incoming flow-sediment condition will slow down or accelerate the bank erosion process. Previous studies have indicated that the flow-sediment condition during flood seasons plays a more important role in the adjustments of channel geometry in LYR (Bi et al., 2019; Li et al., 2021; Xia et al., 2014). Close relations were developed in the literature between bankfull width at section- and reach-scales and the incoming flow-sediment condition (Li et al., 2021; Wu et al., 2008; Xia et al., 2014), which is usually represented by the incoming sediment coefficient during flood seasons ($\xi_{fk} = (\overline{S}_k/\overline{Q}_k)\times 1000$ where $\overline{Q}_k$ and $\overline{S}_k$ are the k years average discharge and sediment concentration during flood seasons). An increase in the incoming sediment coefficient during flood seasons, represents a decrease in flow discharge or an increase in sediment concentration, which furthermore indicates a decrease in stream power. As shown in Fig. 10(b), the relation between the cumulative bank erosion volume and the previous 5-year average incoming sediment coefficient during flood seasons (ξ_{5f}) can be quantified by a logarithmic function with a high coefficient of determination ($R^2 = 0.84$), when the bank erosion volume and ξ_{5f} vary in $(0.05-4.40)\times10^8$ m^3 and $(2.36-54.17)\times10^{-3}$ kg·s/m^6.

4. Quantitative relation between bed incision and bank erosion

On the basis of the calculated results covering bankfull channel dimensions, cumulative bank erosion width, and bed incision depth after reservoir operation, the parameters in Eq. (8) were calibrated. Results are listed in Table 1, which indicate: (i) a negative relation between cumulative bank erosion width and bed incision depth was common in each reach. The bed incision depth increased with K_B in each reach, which indicates that the incision depth decreased with a high degree of bank erosion; (ii) Eq. (8) can well reflect the relation between bank erosion and bed incision, with the coefficient of determination larger than 0.90 in each reach; (iii) the variation rate of bed incision depth with K_B was similar in Reaches R1 and R2, while the variation rate was the highest in Reach R3. The difference indicates that Reach R3 would experience the most prominent bed incision, if K_B varied at the same magnitude in each reach; (iv) the influence of the temporal variation in flow and sediment condition was indirectly reflected by the calibrated coefficients and K_B in different reaches; (v) compared with fully empirical relations obtained from optimum fitting, the coefficient of determination of Eq. (8) was improved by 7%–154%. In addition, it is impossible to obtain universal calculation relations based on fully empirical analyses. Therefore, the proposed relations derived

Table 1
Calibration results of Eq. (8) in different reaches.

Reach	Calibrated Eq. (8)	Coefficient of determination
R1	$\Delta H = 0.875 \ln K_B + \frac{\overline{H}_{bf1}\overline{B}_{bf1}}{\overline{B}_{bf1} + 2\Delta B} - \overline{H}_{bf1} + 6.595$	0.93
R2	$\Delta H = 0.956 \ln K_B + \frac{\overline{H}_{bf1}\overline{B}_{bf1}}{\overline{B}_{bf1} + 2\Delta B} - \overline{H}_{bf1} + 6.715$	0.94
R3	$\Delta H = 1.183 \ln K_B + \frac{\overline{H}_{bf1}\overline{B}_{bf1}}{\overline{B}_{bf1} + 2\Delta B} - \overline{H}_{bf1} + 7.248$	0.95
Braided reach	$\Delta H = 0.995 \ln K_B + \frac{\overline{H}_{bf1}\overline{B}_{bf1}}{\overline{B}_{bf1} + 2\Delta B} - \overline{H}_{bf1} + 6.903$	0.96

from the equation of sediment continuity are more statistically and theoretically accurate.

Fig. 11 shows the comparison between the calculated and observed cumulative bed incision depths in each reach. The corresponding data in 2018–2020 were used to verify the accuracy of Eq. (8). The results calculated using Eq. (8) can well reproduce and predict the variation in the cumulative bed incision depth in each reach. The relative error of the predicted bed incision depth in each reach varied from 0.9% to 49.3% during the period of 2018–2020. The discrepancy mainly occurred in 2019, when all the predicted bed incision depths greatly deviated from the observed values in each reach except Reach R3. The significant channel deposition in this year as previously mentioned contributed to the error. The calibrated results were obtained using the measurements under the state of continuous and considerable channel scour, which failed to give accurate predictions under the state of significant channel deposition. These quantitative relations can well predict the bed incision depth under the state of channel degradation, with the relative errors lower than 10% in 2018 and 2020 in each reach. Therefore, the proposed quantitative relations more reasonably reflect the variation in bank erosion width and bed incision depth of a reach undergoing continuous channel degradation.

If there was no bank erosion after 1999, assuming that the developed relations are still applicable, the temporal variation in cumulative bed incision depth in each reach is shown in Fig. 11. It is obvious that the bed incision depth would increase without bank erosion, and the cumulative depth of bed incision would be equal to 3.16 m in Reach R1, 2.90 m in Reach R2, 3.26 m in Reach R3, and 3.12 m in the braided reach during the period of 1999–2020. It could be concluded that the cumulative bed incision depth would increase by at least 0.69 m compared with the current bed incision depth in each reach over the past 20 years. Therefore, it is verified again that the bed incision process was hindered by the considerable bank erosion.

To further verify the applicability of the proposed relations (Eq. (8)), the measured cross-sectional profiles in the braided reach were collected during the period of 1960–1964. Significant changes occurred in the flow-sediment regime and channel boundary conditions after 1960, and therefore, this verification case can be regarded as a further application in a totally new braided reach. This period was characterized by abundant incoming water discharge and low sediment load due to the powerful trap efficiency of the SMX Reservoir at its first operation stage (Fig. 2(a)). As a consequence, the channel in LYR experienced severe degradation, with a cumulative scour volume of 15.21×10^8 m^3 in the braided reach (Fig. 2(b)). The processes of bank erosion and bed incision were prominent in the braided reach, with the reach-scale bankfull width and depth increasing by 570 and 0.61 m, respectively, in these four years (Fig. 12(a)). The average annual bank erosion width was around 143 m/y, which was much more than that after the operation of XLD Reservoir (20 m/y). The differences could be attributable to the reduced water and sediment amount together with the improved bank protection works after the operation of the XLD Reservoir. The variations in cumulative bed incision depth

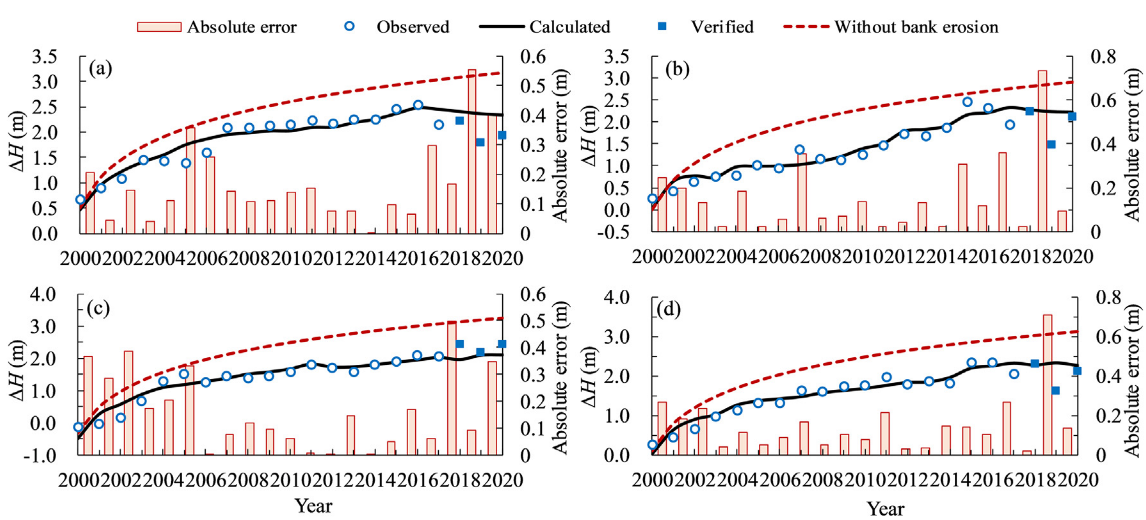

Fig. 11. Comparisons between calculated and observed cumulative bed incision depths in different reaches.

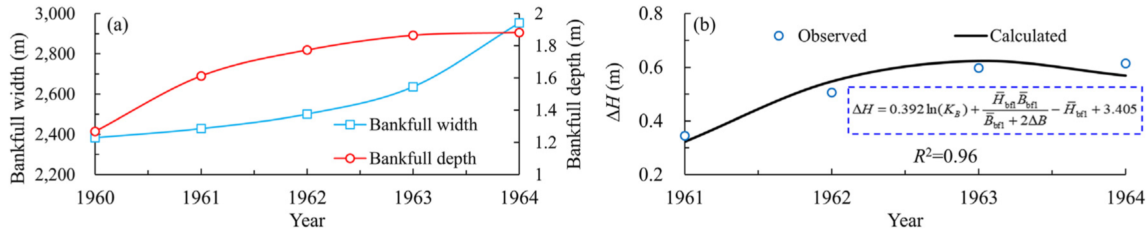

Fig. 12. Variation in bank erosion and bed incision in the braided reach during the first operation stage of SMX Reservoir (1960–1964): (a) temporal variations in bankfull width and depth and (b) comparison between calculated using Eq. (8) and observed cumulative bed incision depths.

during this period can be also well reproduced using Eq. (8). As shown in Fig. 12(b), the calculated bed incision depth was in close agreement with the observed values, with the coefficient of determination being equal to 0.96. As the process of bank erosion was gradually dominant in the reach, the increase in the bed incision depth became relatively slow, which was reflected by the gradually flatter curve.

The incoming water and sediment amounts were the largest in 1964, with values of 823 $\times$ 10^8 m^3 and 14.6$\times 10^8$ t. The bankfull width significantly increased by 317 m in this year, which was three times the value of other years. As a result, the cumulative bed incision depth was not well calculated based on Eq. (8) in this year. The proposed relation could reflect the general variation in bed incision depth, which may not be able to accurately consider the abrupt variation in a specified year with the flow-sediment regime greatly deviating from the general range. In general, this validation case indicates that the quantitative relation derived from the equation of sediment continuity could be applicable to other sand-bed braided rivers with regular measurements of cross-sectional topography, which also underwent continuous channel degradation, although some necessary simplifications are made.

In summary, the morphological changes of downstream reaches in response to upstream damming are significant. Channel evolution is the result of the interaction between sediment-laden flow, and the erodible river bed and banks. Channel degradation definitely occurred due to the considerably reduced sediment load and slightly changed water volume. For a braided river with erodible bank material, both bank erosion and bed incision occurred concurrently. Around 33% of the total channel evolution volume was supplied from the river banks in the braided reach of LYR after the operation of XLD Reservoir, which would not only greatly influence the sediment transport process but also the channel adjustment process. Therefore, the quantitative relation between bank erosion and bed incision was deduced based on the sediment continuity equation and large-scale cross-section measurements, with quite high accuracy during different study periods. Although some deviations existed in the calculated bed incision depth when the river experienced channel aggradation, the proposed method demonstrated an accurate quantification of the internal relation between bank erosion and bed incision. This approach is also applicable to other braided rivers undergoing channel incision and widening.

5. Conclusions

The phenomena of bank erosion and bed incision are prevalent in fluvial processes of the braided reach of LYR especially during the post-dam operation stage. A comprehensive investigation has been done into the magnitude and effect of bank erosion in the braided reach. A method based on the measured cross-sectional profiles was proposed to estimate the bank erosion volume. Then the effect of bank erosion on the bed incision process was revealed on the basis of the sediment continuity equation. The main findings of the current study are obtained as follows:

(1) The channel adjustment characteristics have been revealed, with the reach-scale bankfull channel dimensions obtained in different reaches. The phenomena of bank erosion and bed incision were dominant in the fluvial processes of the braided reach. The bankfull width increased by 48% in Reach R1, 38% in Reach R2, 52% in Reach R3, and 45% in the braided reach after the operation of the XLD Reservoir, and in the meantime the bankfull depth increased by 130%, 154%, 124%, and 136% in different reaches, respectively. Bank erosion was dominant over accretion at more than 71% of the cross-sections in the braided reach. The highest erosion and accretion activities were detected in Reach R2, with the values of erosion and accretion widths exceeding 1000 m.

(2) The cumulative bank erosion volumes in the different reaches have been estimated, with the contribution to the channel evolution volume determined. A gradual increase commonly existed in the cumulative bank erosion volume of each reach, with the total value of 1.80$\times 10^8$ m^3 in Reach R1, 1.52$\times 10^8$ m^3 in Reach R2, 1.08$\times 10^8$ m^3 in Reach R3, and 4.40$\times 10^8$ m^3 in the braided reach. The sediment from bank erosion contributed to 33% of the channel scour volume during the period of 1999–2020, which indicated that bank erosion played an important role in the fluvial processes of the braided reach.

(3) A quantitative relation between bed incision depth and bank erosion width was deduced from the sediment continuity equation, which was further calibrated and verified using the measurements in different periods. Negative relations were proven to exist between cumulative bed incision depth and bank erosion width in different reaches, with the coefficients of determination larger than 0.90, which indicated that bank erosion hindered the process of bed incision. If there was no bank erosion after 1999, the cumulative bed incision depth in the braided reach would increase by at least 0.7 m compared with the current values. Furthermore, quite high accuracy was found in the calculated cumulative bed incision depth of the braided reach during the period of 1960–1964 (the first stage after the SMX Reservoir operation) using this similar quantitative relation, with the coefficient of determination being equal to 0.96.

Declaration of competing interest

The authors declare that they have no known competing financial interests or personal relationships that could have appeared to influence the work reported in this paper.

CRediT authorship contribution statement

Junqiang Xia: Supervision, Resources, Methodology, Investigation, Funding acquisition. **Yifei Cheng:** Writing – review & editing, Writing – original draft, Methodology. **Meirong Zhou:** Writing – review & editing, Validation, Formal analysis. **Xin Yu:** Writing – review & editing, Validation. **Xiangzhou Xu:** Writing – review & editing, Validation. **Koen Blanckaert:** Writing – review & editing, Validation, Formal analysis. **Zhengbing Wang:** Writing – review & editing.

Acknowledgements

The work was supported by the National Natural Science Foundation of China (Grant No. U2243238), the Program of the National Key Research and Development Plan (Grant No. 2023YFC3209304), and the National Natural Science Foundation of China (Grant No. U2243237).

References

Arnez Ferrel, K. R., Patsinghasanee, S., Kimura, I., & Shmizu, Y. (2018). Coupled model of bank erosion and meander evolution for cohesive riverbanks. *Geosciences, 8*(10), 359.
Asahi, K., Shimizu, Y., Nelson, J., & Parker, G. (2013). Numerical simulation of river meandering with self-evolving banks. *Journal of Geophysical Research-Earth Surface, 118*(4), 2208–2229.
Basumatary, H., Sah, R. K., & Das, A. K. (2021). Bankline dynamics and their effects on protected areas along the Brahmaputra river. *Catena, 197*, 104947.
Bi, N. S., Sun, Z. Q., Wang, H. J., Wu, X., Fan, Y. Y., Xu, C. L., & Yang, Z. S. (2019). Response of channel scouring and deposition to the regulation of large reservoirs: A case study of the lower reaches of the Yellow River (Huanghe). *Journal of Hydrology, 568*, 972–984.
Boardman, J. (2016). The value of Google EarthTM for erosion mapping. *Catena, 143*, 123–127.
Brandt, S. A. (2000). Classification of geomorphological effects downstream of dams. *Catena, 40*(4), 375–401.
Craddock, W. H., Kirby, E., Harkins, N. W., Shi, X. H., & Liu, J. H. (2010). Rapid fluvial incision along the Yellow River during headward basin integration. *Natural Geoscience, 3*(3), 209–213.
Darby, S. E., Rinaldi, M., & Dapporto, S. (2007). Coupled simulations of fluvial erosion and mass wasting for cohesive river banks. *Journal of Geophysical Research-Earth Surface, 112*(F3), F03022.
Deng, S. S., Xia, J. Q., Liu, X., Zhou, M. R., Mao, Y., & Xu, Q. X. (2022). Contributions of different sources to sediment transport in the Middle Yangtze River under intensive channel degradation. *Catena, 217*, 106511.
Deng, S. S., Xia, J. Q., Zhou, M. R., & Lin, F. F. (2019). Coupled modeling of bed deformation and bank erosion in the Jingjiang Reach of the middle Yangtze River. *Journal of Hydrology, 568*, 221–233.
Fisher, G. B., Bookhagen, B., & Amos, C. B. (2013). Channel planform geometry and slopes from freely available high-spatial resolution imagery and DEM fusion: Implications for channel width scalings, erosion proxies, and fluvial signatures in tectonically active landscapes. *Geomorphology, 194*, 46–56.
Florsheim, J. L., Mount, J. F., & Chin, A. (2008). Bank erosion as a desirable attribute of rivers. *BioScience, 58*(6), 519–529.
Fox, G. A., Purvis, R. A., & Penn, C. J. (2016). Streambanks: A net source of sediment and phosphorus to streams and rivers. *Journal of Environmental Management, 181*, 602–614.
Harman, C., Stewardson, M., & Derose, R. (2008). Variability and uncertainty in reach bankfull hydraulic geometry. *Journal of Hydrology, 351*(1–2), 13–25.
Huang, H. Q., & Nanson, G. C. (2000). Hydraulic geometry and maximum flow efficiency as products of the principle of least action. *Earth Surface Processes and Landforms, 25*(1), 1–16.
Hyndman, R. J., & Athanasopoulos, G. (2018). *Forecasting: Principles and practice* (2nd ed.). Melbourne, Australia: OTexts.com/fpp2.
Klavon, K., Fox, G., Guertault, L., Enlow, H., Miller, R., & Khanal, A. (2017). Evaluating a process-based model for use in streambank stabilization: Insights on the bank stability and toe erosion model (BSTEM). *Earth Surface Processes and Landforms, 42*, 191–213.
Lane, E. W. (1955). The importance of fluvial morphology in hydraulic engineering. *Proceedings of the American Society of Civil Engineers, 81*, 1–17.
Latrubesse, E. M., Arima, E. Y., Dunne, T., Park, E., Baker, V. R., D'Horta, F. M., Wight, C., Wittmann, F., Zuanon, J., Baker, P. A., Ribas, C. C., Norgaard, R. B., Filizola, N., Ansar, A., Flyvbjerg, B., & Stevaux, J. C. (2017). Damming the rivers of the Amazon basin. *Nature, 546*(7658), 363–369.
Leopold, L. B., & Maddock, T. (1953). *The hydraulic geometry of stream channels and some physiographic implications*. U.S. Geological Survey.. Professional Paper No. 252.
Leyland, J., Christopher, R. H., Darby, S. E., Parsons, D. R., Best, J. L., Nicholas, A. P., Aalto, R., & Lague, D. (2017). Extreme flood-driven fluvial bank erosion and sediment loads: Direct process measurements using integrated mobile laser scanning (MLS) and hydro-acoustic techniques. *Earth Surface Processes and Landforms, 42*, 334–346.
Li, J., Xia, J. Q., & Ji, Q. F. (2021). Rapid and long-distance channel incision in the Lower Yellow River owing to upstream damming. *Catena, 196*, 104943.
Ma, Y. X., Huang, H. Q., Nanson, G. C., Li, Y., & Yao, W. Y. (2012). Channel adjustments in response to the operation of large dams: The upper reach of the lower Yellow River. *Geomorphology, 147–148*(1–4), 35–48.
Meade, R. H., & Moody, J. A. (2010). Causes for the decline of suspended-sediment discharge in the Mississippi River system, 1940–2007. *Hydrological Processes, 24*, 35–49.
Miao, C. Y., Kong, D. X., Wu, J. W., & Duan, Q. Y. (2016). Functional degradation of the water-sediment regulation scheme in the lower Yellow River: Spatial and temporal analyses. *Science of the Total Environment, 551–552*, 16–22.
Millar, R. G. (2005). Theoretical regime equations for mobile gravel-bed rivers with stable banks. *Geomorphology, 64*, 207–220.
Nandi, K. K., Pradhan, C., Padhee, S. K., Dutta, S., & Khatua, K. K. (2022). Understanding the entropy-based morphological variability and energy expenditure mechanism of a large braided river system. *Journal of Hydrology, 615*, 128662.
O'Neal, M. A., & Pizzuto, J. E. (2011). The rates and spatial patterns of annual riverbank erosion revealed through terrestrial laser-scanner surveys of the South River, Virginia. *Earth Surface Processes and Landforms, 36*, 695–701.
Payne, C., Panda, S., & Prakash, A. (2017). Remote sensing of river erosion on the Colville river, North Slope Alaska. *Remote Sensing, 10*, 397.
Richard, G. A., Julien, P. Y., & Baird, D. C. (2005). Case study: Modeling the lateral mobility of the Rio Grande below Cochiti dam, New Mexico. *Journal of Hydraulic Engineering, 131*(11), 931–941.
Rowland, J. C., Shelef, E., Pope, P. A., Muss, J., Gangodagamage, C., Brumby, S. P., & Wilson, C. J. (2016). A morphology independent methodology for quantifying planview river change and characteristics from remotely sensed imagery. *Remote Sensing of Environment, 184*, 212–228.
Słowik, M., Dezső, J., Marciniak, A., Tóth, G., & Kovács, J. (2018). Evolution of river planforms downstream of dams: Effect of dam construction or earlier human induced changes? *Earth Surface Processes and Landforms, 43*(10), 2045–2063.
Shin, Y. H., & Julien, P. Y. (2010). Changes in hydraulic geometry of the Hwang river below the Hapcheon Re-regulation dam, South Korea. *International Journal of River Basin Management, 8*(2), 139–150.
Spiekermann, R., Betts, H., Dymond, J., & Basher, L. (2017). Volumetric measurement of river bank erosion from sequential historical aerial photography. *Geomorphology, 296*, 193–208.
Swanson, B. J., Meyer, G. A., & Coonrod, J. E. (2011). Historical channel narrowing along the Rio Grande near Albuquerque, New Mexico in response to peak discharge reductions and engineering: Magnitude and uncertainty of change from air photo measurements. *Earth Surface Processes and Landforms, 36*, 885–900.
Walling, D. E., & Fang, D. (2003). Recent trends in the suspended sediment loads of the world's rivers. *Global and Planetary Change, 39*, 111–126.
Wang, H. J., Wu, X., Bi, N. S., Li, S., Yuan, P., Wang, A., Syvitski, J. P. M., Saito, Y., Yang, Z. S., Liu, S. M., & Nittrouer, J. (2017). Impacts of the dam-orientated water-sediment regulation scheme on the lower reaches and delta of the Yellow River (Huanghe): A review. *Global and Planetary Change, 157*, 93–113.
Wang, Y. Z., Xia, J. Q., Deng, S. S., Zhou, M. R., Wang, Z. H., & Xu, X. Z. (2022). Numerical simulation of bank erosion and accretion in a braided reach of the Lower Yellow river. *Catena, 217*, 106456.
Wilkerson, G. V., Kandel, D. R., Perg, L. A., Dietrich, W. E., Wilcock, P. R., & Whiles, M. R. (2014). Continental-scale relationship between bankfull width and drainage area for single-thread alluvial channels. *Water Resources Research, 50*(2), 919–936.
Williams, F., Moore, P., Isenhart, T., & Tomer, M. (2020). Automated measurement of eroding streambank volume from high resolution aerial imagery and terrain analysis. *Geomorphology, 367*, 107313.

Winters, P. R. (1960). Forecasting sales by exponentially weighted moving averages. *Management Science, 6*(3), 324–342.

Wu, B. S., Xia, J. Q., Fu, X. D., Zhang, Y. F., & Wang, G. Q. (2008). Effect of altered flow regime on bankfull area of the Lower Yellow River, China. *Earth Surface Processes and Landforms, 33*, 1585–1601.

Xia, J. Q., Li, X. J., & Li, T. (2014). Response of reach-scale bankfull channel geometry to the altered flow and sediment regime in the lower Yellow River. *Geomorphology, 213*, 255–265.

Xia, J. Q., Wu, B. S., Wang, Y. P., & Zhao, S. G. (2008). An analysis of soil composition and mechanical properties of riverbanks in a braided reach of the Lower Yellow River. *Chinese Science Bulletin, 53*(15), 2400.

Xu, J. X., & Shi, C. X. (1995). Bank erosion in the braided reach downstream of the Danjiangkou Reservoir and its implication in the channel adjustment. *Chinese Science Bulletin, 40*(18), 1689–1692. *(in Chinese)*

Yan, G., Cheng, H. Q., Jiang, Z. Y., Teng, L. Z., Tang, M., Shi, T., Jiang, Y. H., Yang, G. Q., & Zhou, Q. P. (2023). Recognition of fluvial bank erosion along the main stream of the Yangtze River. *Engineering, 19*, 50–61.

Yang, C., Cai, X. B., Wang, X. L., Yan, R. R., Zhang, T., Zhang, Q., & Lu, X. R. (2015). Remotely sensed trajectory analysis of channel migration in lower Jingjiang reach during the period of 1983–2013. *Remote Sensing, 7*, 16241–16256.

Zhang, Z. D., Shu, A. P., Zhang, K. L., Wang, J., & Dai, J. B. (2019). Quantification of river bank erosion by RTK GPS monitoring: Case studies along the Ningxia–Inner Mongolia reaches of the Yellow River, China. *Environmental Monitoring and Assessment, 191*(3), 140.

Zhou, Z. D. (1992). The relationship between bank erosion and bed incision in the Lower Yellow River during the first stage after the Sanmenxia Reservoir operation releasing clear water. *Yellow River, 6*, 14–15. *(in Chinese)*